CAMECA
SCIENCE & METROLOGY SOLUTIONS

AMETEK

NanoSIMS 50L

Application in Materials

Secondary Ion Mass Spectrometer
for trace element and isotope analysis
at sub-micron resolution



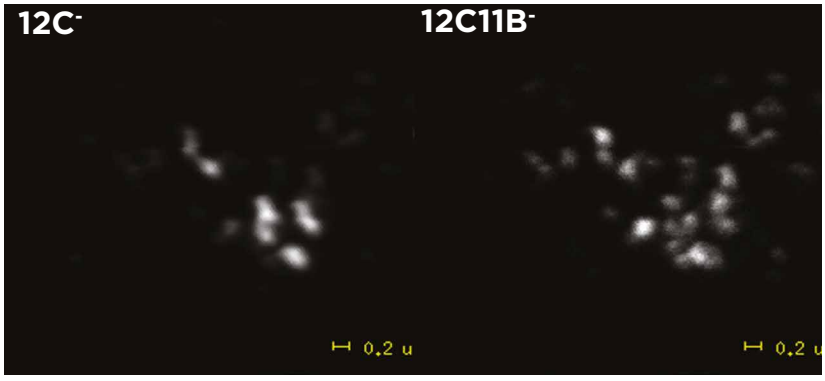
Practical aspects, sensitivity and spatial resolution

Dark spots in silicon nitride Si_3N_4 (1 mm thick)

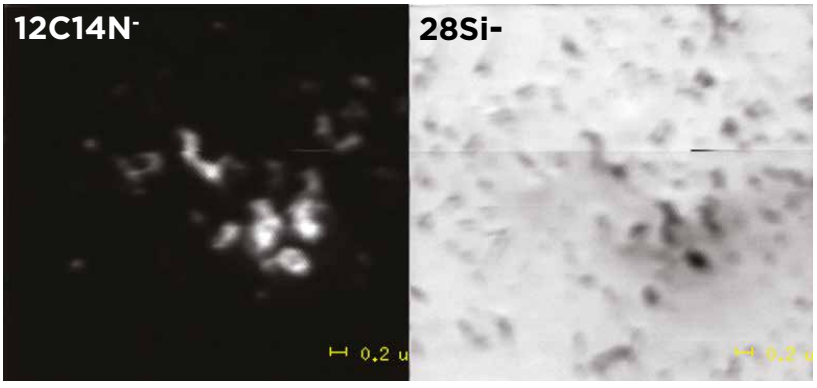
Sample preparation can be difficult with other techniques: TEM can require tedious and not always feasible sample thinning. In contrast, the NanoSIMS analyzes the surface of flat samples (up to several mm thickness and flatness of a few tens microns). In this case, the sample was analyzed as received, 1 mm-thick.

Analysis of bulk strong electrical insulator: FE-Auger was unusable here due to the charging problem. The NanoSIMS analyzes insulators, using when needed a self-adjusting electron flood gun to annihilate charging effects. Metal coating can also be used (a few tens nm of Pt, Au, etc.) to facilitate charge evacuation.

Navigation over large sample: in contrast to TEM the NanoSIMS permits to load samples of cm dimensions and navigate over the sample surface, guided by in-situ optical, secondary electron or SIMS images, and chain image acquisitions over selected FoV typically between 1x1µm and 50x50µm. Larger FoV are recorded in mosaic mode and images are stitched.



Carbon max: 12 900 counts/pixel. Boron max: 247 counts/pixel.



Nitrogen max: 9 470 counts/pixel. Silicon max: 12 000 counts/pixel.

Field of view: 6 µm x 6 µm, Acq time: 22 min., 256 x 256 pixels, 16 keV Cs+ , spot size: 100 nm, Ip: 1.5 pA, M/dM: 5000, parallel acquisition of 4 masses.
Courtesy of G. Barbier, Céramétal, Luxembourg.

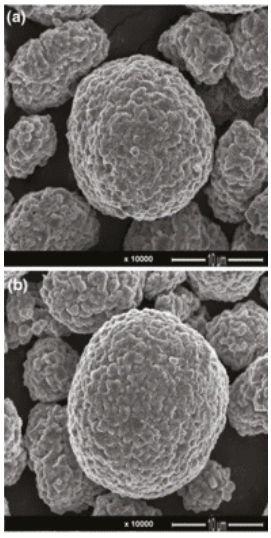
Sensitivity approximation from small area: let's simplify this example and assume that [C] = [N] = [Si] = 100 at%. Counting around 10 000 counts per single pixel on C, N and Si indicates a **detection limit** (at one count) of **hundred ppm range per pixel or a 100nm spot, within 22 min** acquisition time. Summing a few tens pixels from a small area allows to reach **ppm level.**

The NanoSIMS is unique in permitting fast mapping of TRACE elements (including light elements) at hundred nm resolution and with high mass resolution.

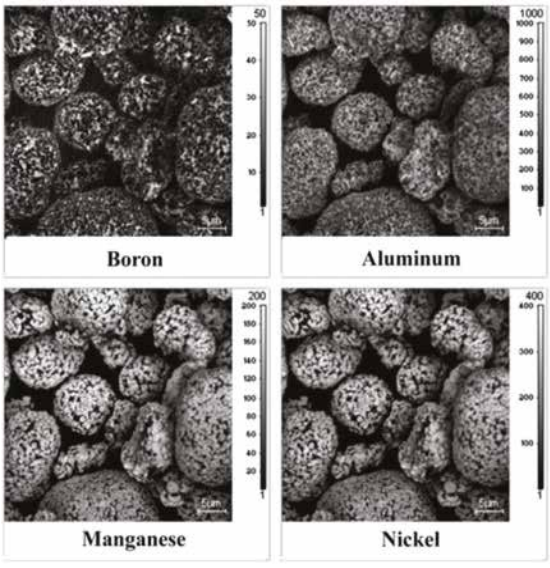
Normal incidence & ion collection for topographical samples

Li-ion battery: B & Al-coated $LiNi_{1/3}Co_{1/3}Mn_{1/3}O_2$ cathode materials

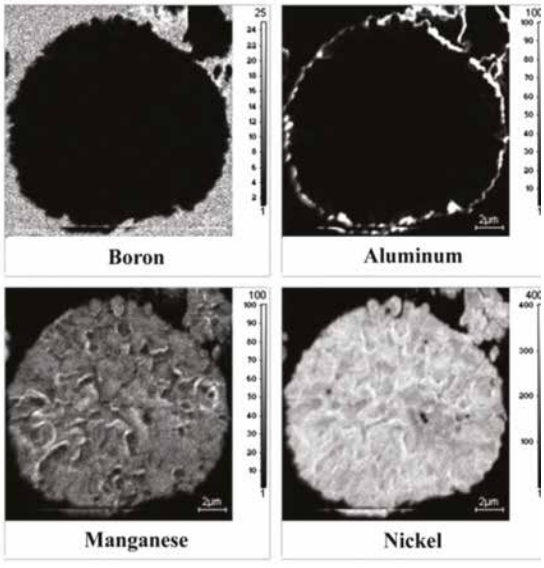
Abstract's extract: "$LiNi_{1/3}Co_{1/3}Mn_{1/3}O_2$ powders obtained by coprecipitation have been surface **coated with B and Al**. TEM & NS50 element maps of the coated samples indicate a thin uniform layer of [B, Al]$_2O_3$ on the surface of spherical $LiNi_{1/3}Co_{1/3}Mn_{1/3}O_2$. Surface-modified $LiNi_{1/3}Co_{1/3}Mn_{1/3}O_2$ has been explored as a cathode material for Li secondary ion batteries. Small amount of B and Al coatings on the surface of $LiNi_{1/3}Co_{1/3}Mn_{1/3}O_2$ can significantly improve the electrochemical properties of electrode materials because of the suppression of reaction between the cathode and the electrolytes...". **Two sample preparations were used: 1)** powder analyzed from the **top surface. 2)** powder mounted using epoxy resin and then polished with SiC paper to measure the element distribution on the **cross section** of the coated $LiNi_{1/3}Co_{1/3}Mn_{1/3}O_2$ powders.



SEM (top: uncoated, bottom: coated



NS50: Surface

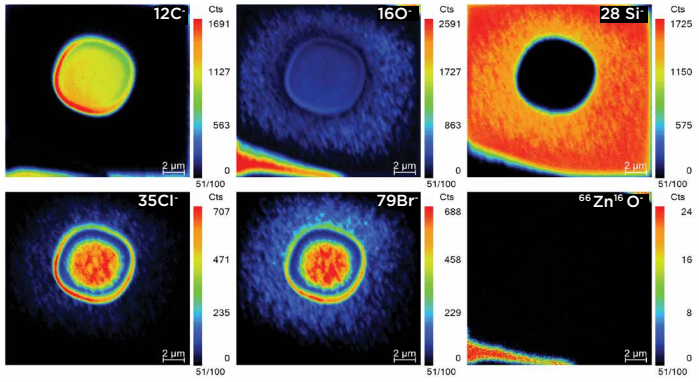


NS50: particle section (20 x 20 µm)

Ni and Mn elements are distributed uniformly throughout the $LiNi_{1/3}Co_{1/3}Mn_{1/3}O_2$ particles as desired. Note the uniform collection and absence of primary shadowing thanks to the normal and co-axial design of NanoSIMS.

From: NanoSIMS characterization of boron- and aluminum-coated $LiNi_{1/3}Co_{1/3}Mn_{1/3}O_2$ cathode materials for lithium secondary ion batteries. Tae Eun Hong et al. J Appl Electrochem (2012) 42:41–46.

Depth profiling inside hole (diam. 7µm, depth 1µm) in display technology



Two analysis modes were used:
1) A stack of 100 images was recorded and a depth profile was reconstructed from a small region of interest drawn in the center of the hole.

2) A direct depth profile was recorded with 3x3µm crater and 2x2µm gate in the center of the hole.
The first method gives an overview and more control while the second is faster.
Uniquely, the normal and co-axial NS50L geometry with single ion gun approach make such analysis possible.

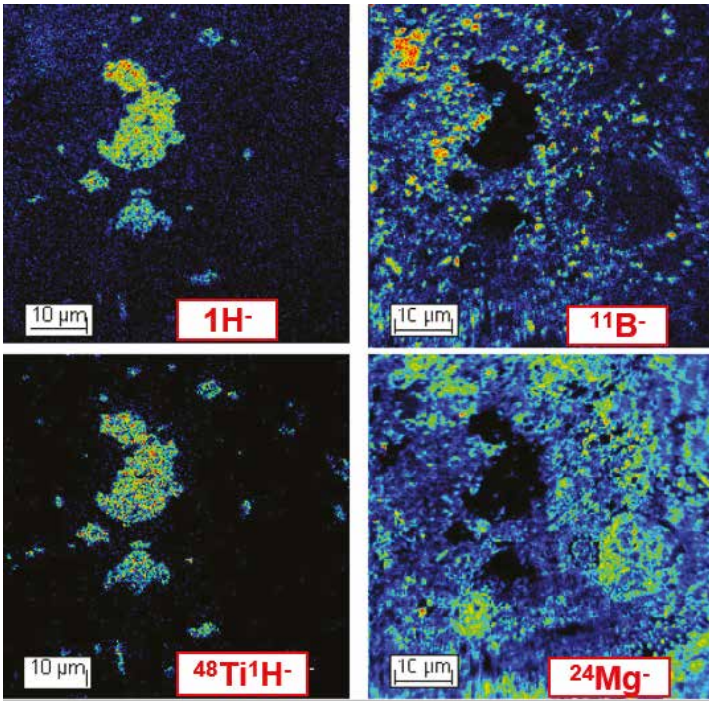
The normal primary ion incidence with co-axial ion collection permits a uniform collection from samples with topography without shadowing or loss of sensitivity.

Analysis of hydrogen with high lateral resolution

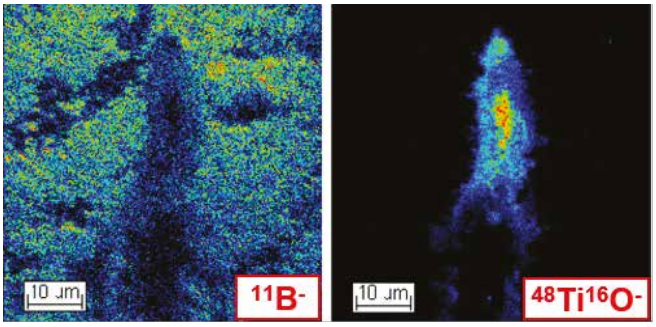
Chemical interactions in Ti-doped MgB_2 superconductor

MgB_2 superconducting wires and bulk samples synthesized at high pressure have been produced with a variety of reactive metal additions. All these samples showed high critical current densities. Reactive metal additions such as titanium substantially improved the critical current values, but had little detrimental effect on Tc values. (...) In a detailed study of the microstructure of these materials we have shown that PIT ex situ wires with 10 wt% titanium additions have a complicated layered microstructure around the Ti-rich particles, possibly forming titanium–boron phases, but also incorporating impurity elements including hydrogen. XRD data, TEM and elemental mapping in the NanoSIMS confirmed the surprising suggestion that samples synthesized at high pressure from Mg and B with Ti additions contain a titanium hydride...."

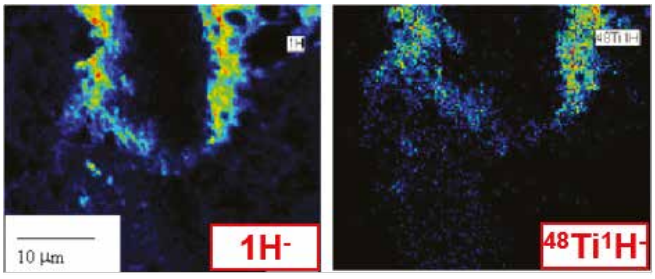
The NanoSIMS is used below to map hydrogen and titanium hydride in parallel with major elements:



Pressure synthesized MgB_2 bulk material with 10 wt% Ti additions: presence of hydrides.



PIT ex situ wire with 10 wt% Ti addition. The TiO ion image shows the position of the spongy Ti particle with O-rich core but some enhanced signal from the surrounding Ti-rich region as well.



Area of the PIT ex situ wire with 10 wt% Ti addition containing one spongy Ti particle

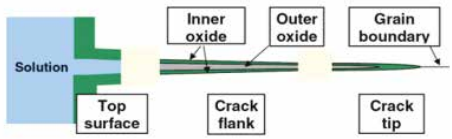
A detailed study of the chemistry of Ti additions to two kinds of MgB_2 materials can reveal the interaction of light elements with the reactive metal particles: in hot-pressed bulk material the primary interaction is confirmed to be the formation of TiH1.924, while in the ex situ processed wire Ti seems to absorb oxygen and hydrogen as well as reacting with boron from the core. These new data strongly support the theory that the **primary role of Ti in improving the superconducting properties of MgB_2 is the absorption of deleterious impurities from the superconducting matrix.** This also helps explain why any reactive metal will have a similar beneficial effect, since similar chemical interactions might be expected with all these additions. A 2nd advantage of the addition of metallic particles may be the reduction in normal state resistivity in the core..."

From: Chemical interactions in Ti doped MgB2 superconducting bulk samples and wires. S. Haigh, PKovac, T.A. Prikhna, Ya. M. Savchuk, M. R. Kilburn, C. Salter, J. Hutchison and C. R. M. Grovenor. Supercond. Sci. Technol. 18 (2005) 1190–1196.

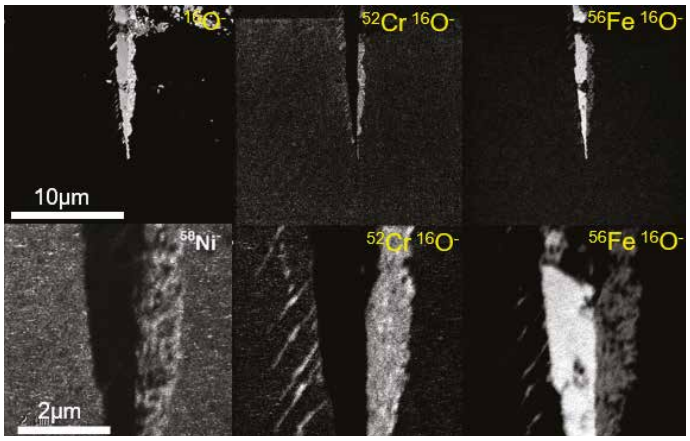
The NanoSIMS works under UHV with a DC primary Cs^+ beam. This permits hydrogen measurements with low background, not accessible with TOF-SIMS, and down to 50nm resolution, not accessible with conventional Mag-SIMS.

Oxide formation and cracks in nuclear reactor steel

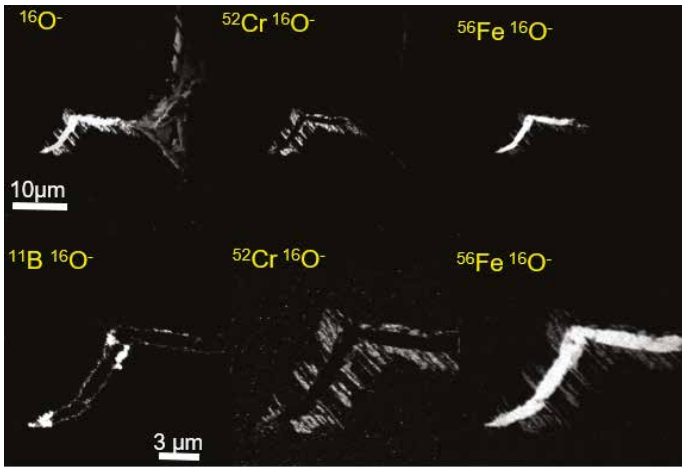
Oxide formation in a growing crack tip



Stress corrosion crack and its representative features.



CrO and FeO images clearly illustrate segregation of the oxide phases. It is possible to see the oxide penetrating along crystallographic shear bands into adjacent grain. This appears to occur only where the crystallographic grain orientation is favorable. The Fe-oxide is associated with this side of the crack and the Cr-oxide also penetrates along the shear bands.

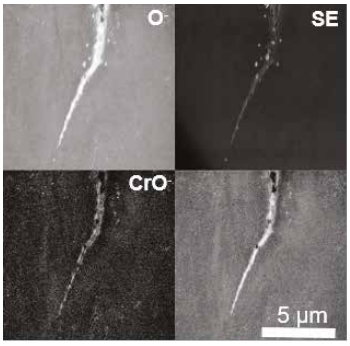


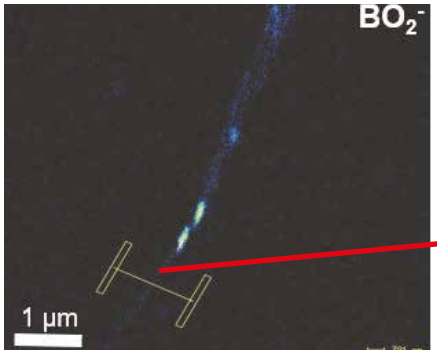
Another crack with oxide penetration along slip planes, on both sides of the crack. Cr-oxide is present only in the slip planes. It is not well understood why cracks favor one GB over another during their propagation. It is possible that the widening of the crack is associated with ingress of oxide along slip planes where the crystallographic orientation is favorable

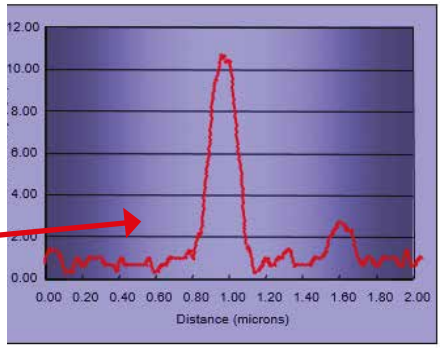
From: High-resolution imaging of complex crack chemistry in reactor steels by NanoSIMS. S. Lozano-Perez, M.R. Kilburn, T. Yamada, T. Terachi, C.A. English, C.R.M. Grovenor. J. Nucl. Mater. (2007).

Segregations at grain boundaries (GB) and crack tips

Impurities in metallic alloys, such as boron, segregate to the grain boundaries (GB). The link between local boundary chemistry and the path along which stress corrosion cracks propagate has been an active area of study for many decades. The chemical and physical processes in front of the crack. A crack tip is shown on the left, in which Cr oxide lines the crack surrounding Fe oxide within. A band scan ahead of the crack tip clearly shows elevated levels of boron oxide, which may be a direct observation of B segregation. In contrast, elevated levels of Cr and Fe oxide are not seen on the GB.







From: M.R. Kilburn, S. Lozano-Perez, C.A. English, C.R.M. Grovenor, Oxford University, poster for SIMS Europe 2006.

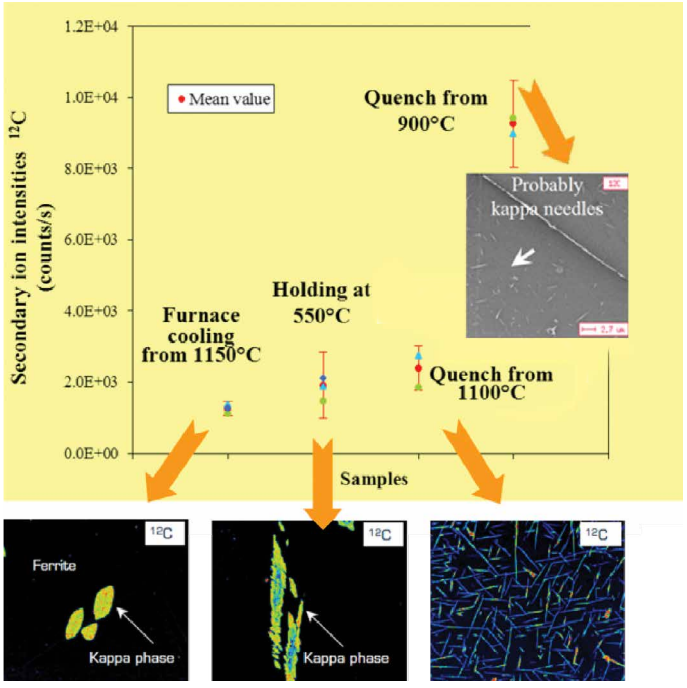
In order to obtain statistically meaningful information from many crack tips optical microscopy, SEM and NanoSIMS are combined, allowing navigation between many spots. Lower throughput TEM or APT can then be applied on a few selected areas.

Low levels of carbon and boron in steel

Fe-Al-Mn-C alloys: reducing the carbon level in ferrite

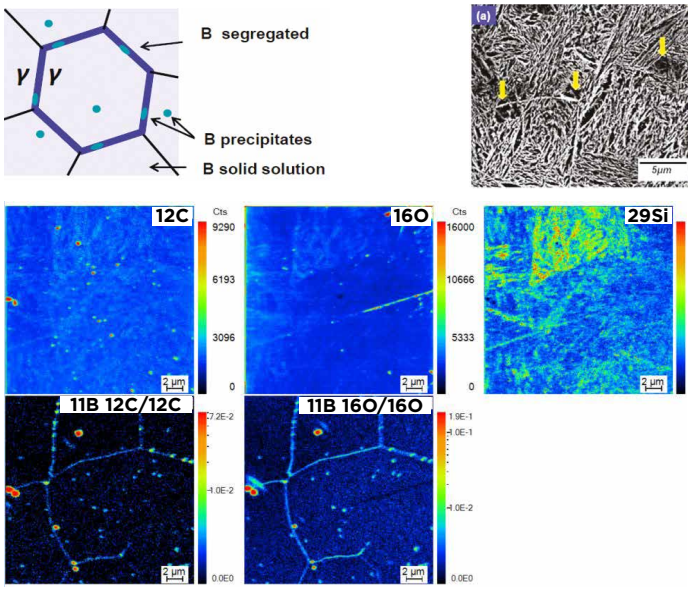
From the abstract: One of the reasons for brittleness of Fe–Al–Mn–C alloys developed at ArcelorMittal is the content of carbon in ferrite. The carbon in solid solution is detrimental to ductility because the C atoms are assumed to reduce the mobility of the edge dislocations. This dislocation pinning produces a twinning mechanism and leads to fracture.
In order to reduce the brittleness of these materials through the reduction of the carbon in solid solution in the ferrite, experimental measurements of the low carbon level (below 0.05 wt%) was done using SIMS. The carbon distribution has been investigated on a Fe–Al–Mn–C grade after different thermal treatments (water quench and slow cooling rate). The NanoSIMS is a well-suited tool to analyze the carbon in solid solution in the ferrite. On the basis of these analyses, it was possible to define thermal treatment conditions necessary to improve the ductility of the material.

From: Application of SIMS nano-analysis to the development of new metallurgical solutions. N. Valle, J. Drillet, A. Perlade and H.-N. Migeon. Applied Surface Science 255 (2008).



Precipitation of boron in steels

Example 1: Synoptic below: boron distribution in steel. Below right: SEM image of HSLA steels containing 50 ppm of boron showing tempered martensite and precipitates along austenite GB.

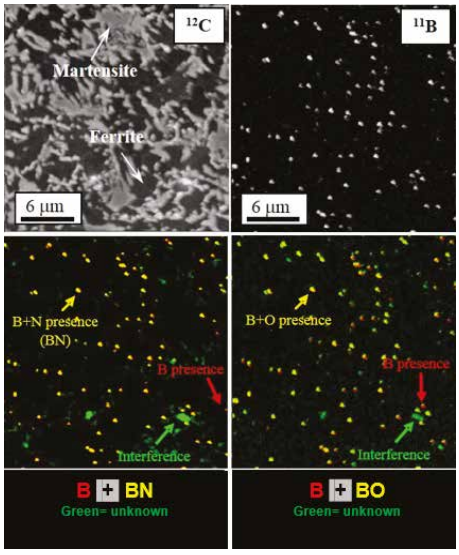


From: APT and NanoSIMS investigation of the segregation of boron at Austenite grain boundaries in 0.5wt% carbon steels. J.B. Seol et al. Met. Mater. Int., Vol 17, N° 3 (2011).

Example 2: Study of the steps of B precipitation during industrial processes of steel (deformation at high temperature, cooling, welding). Parallel detection: B, C, BC, BN & BO.

Boron & carbon distribution in a softened weld area.

In case of mass interference, 11B ion map is overlaid with maps at 25 and 27amu: most boron precipitates contain N and O.

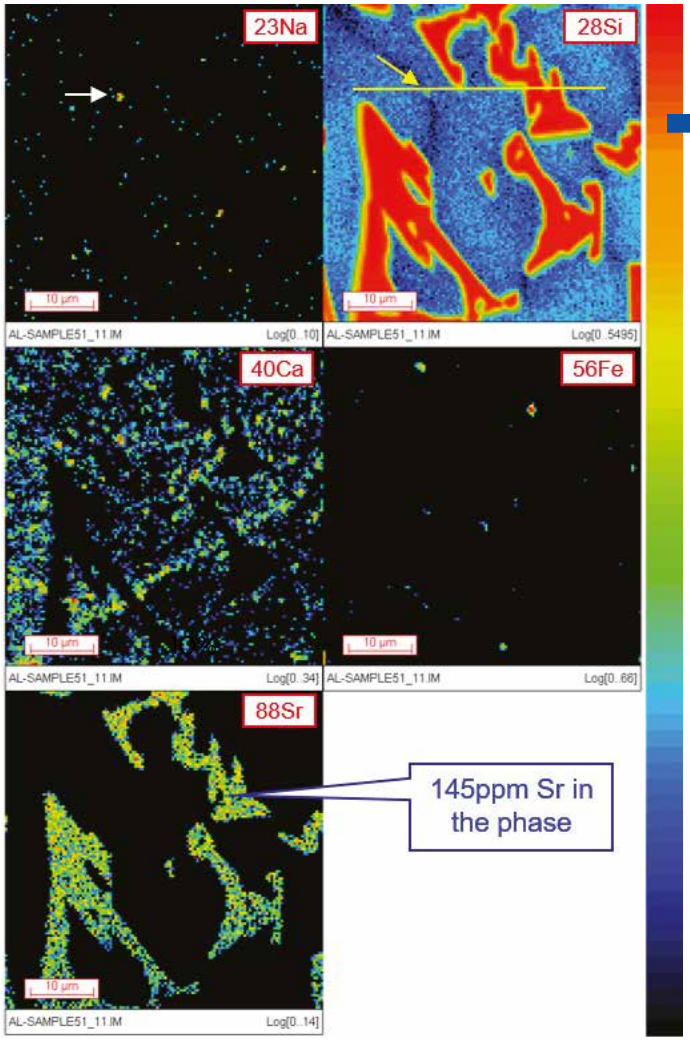


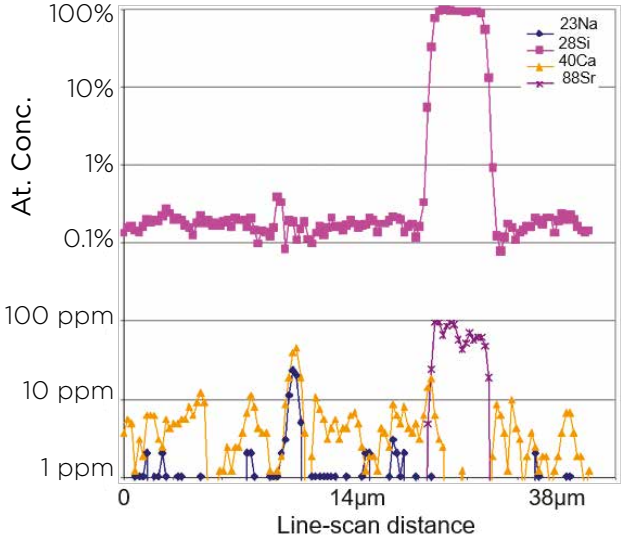
From: NanoSIMS investigation of boron distribution in steels. N. Valle et al., Surface and Interface analysis 2011, 43.

The NanoSIMS offers unique capabilities for steel studies: a) access to the microstructure within a few minutes with elemental and SEM images; b) excellent sensitivity & low background for light element mapping

Quantitative elemental mapping in aluminium alloys

Analysis of electropositive elements

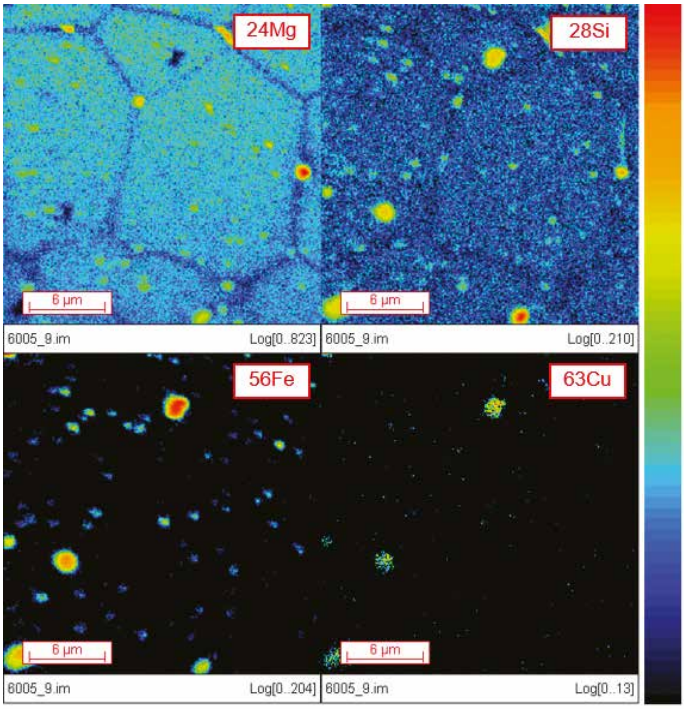




Aluminium alloy containing in average: 7.2wt% Si, 0.1wt% Fe, 0.5wt% Mg, 0.07wt% Cu, 35ppm P, 9ppm Sr, 5.4ppm Ca, < 1ppm Na.
Field: 50 x 50µm, **Acq: 3 min**., O- 16 keV, Ib: 19pA,
Ø: 1µm, 128 x 128 pixels, log. color scale.

A line-scan (shown on 28Si image) is extracted from the image set and displayed on the right side. Note especially the dynamic range between 1ppm and 100at% with an image acquisition time of 3 minutes only, a trademark of the NanoSIMS.

SIMS quantification always requires standards. Here the line-scan quantification was performed by re-injecting RSF derived from larger phase analysis by EPMA.



Aluminium alloy containing in average 0.5wt% Mg, 0.5wt% Si, 0.2wt% Fe, < 0.1wt% Cu and Mn.
Field: 25 x 25µm, Acq: 44min., O- 16 keV, Ib: 0.65pA, Ø: 400nm, 256 x 256 pixels, log. color scale.

Courtesy Dr. Christian J. Simensen, SINTEF materials Technology, Oslo, Norway; Cooperation between SINTEF, ELKEM and CAMECA.

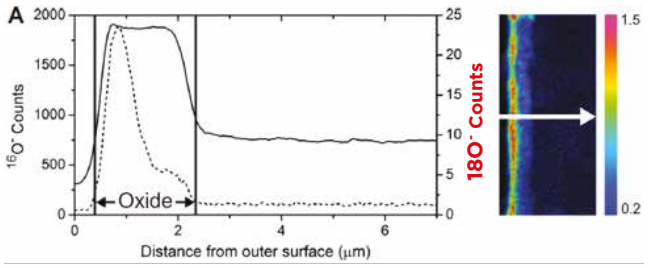
The NanoSIMS offers a high dynamic range in imaging mode. By selecting Cs^+/ negative ions or O^-/ positive ions the NS50L can analyze elements from H up to Pu (except noble gases), down to a lateral resolution of 50nm.

Investigation of the multi-step oxidation behavior of zirconium alloys using isotopic tracers

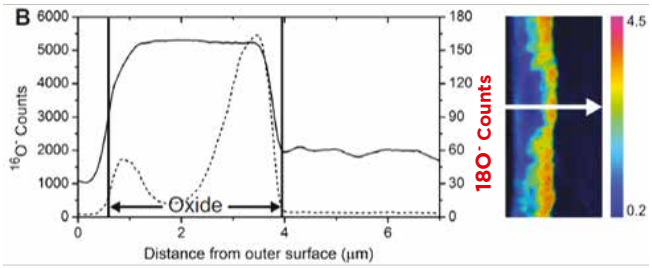
Low tin ZIRLO samples were oxidized in pure water (+ Li, B) at **360°C and 18 MPa for 34, 80 or 160 days** simulating conditions of a nuclear pressurized nuclear reactor. A second, **shorter** oxidation during **20 days** was **then** performed using the same conditions but in **labeled water**: **5% $^{18}O/^{16}O$ and 5% $^{2}H/^{1}H$** in order to reveal active oxidation sites.

Polished sections of the surface were imaged in the NS50, giving a direct view of the oxidation mechanism. Below: typical line scans extracted from images indicating the relative locations of the **^{16}O signal (solid lines) and ^{18}O peaks (dashed lines)**. Image FOV: 15 x 3 µm; band scan length: 7x3µm (white arrows).

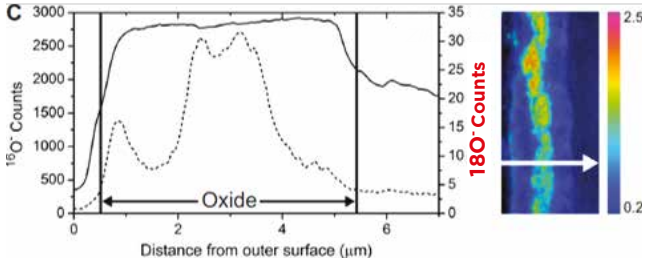
$^{18}O/^{16}O$ ratio images in HSI scale in % (blue: natural isotope ratio (0.2%); pink: highest ratio in that image.



(A) 34 + 20 day sample: Protective oxide! The labeled water could not reach the metal surface, protected by the 34-days oxide



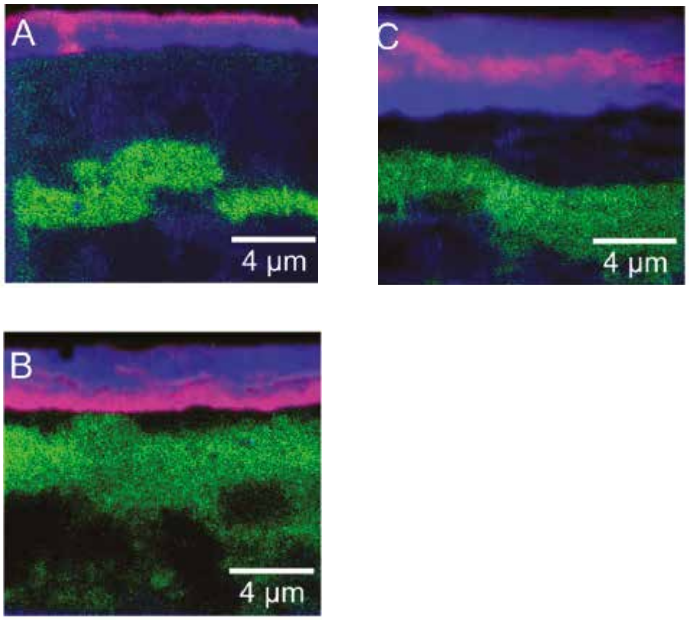
(B) 80 + 20 day sample: too thick, Porous oxide ! Labeled water could reach the metal through the 80 day porous, cracked oxide and create a new oxide layer

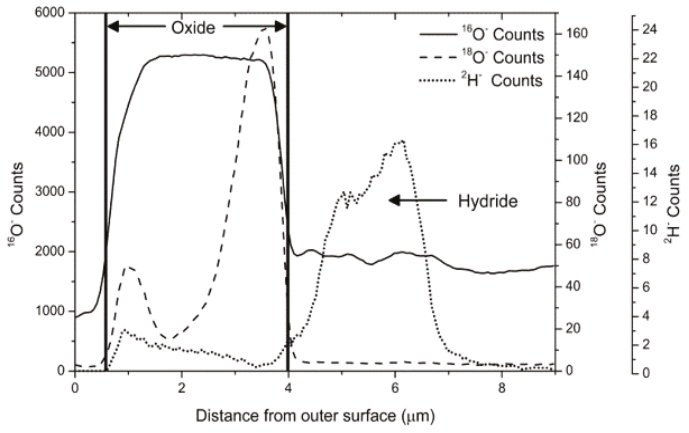


(C) 160 + 20 day sample: New Protective oxide! The labeled water could diffuse through the first porous, cracked oxide but was blocked by the more recent oxide layer.

Below: Colour merge images showing the locations of the **^{18}O (red), ^{16}O (blue) and ^{2}H (green)** signals. **Hydrides** are found below the metal/oxide interface but little deuterium was detected in the oxide layer.

(A) 34 + 20 day low tin ZIRLO sample, **(B) 80 + 20 day** low tin ZIRLO sample, and **(C) 160 + 20 day** low tin ZIRLO sample. Hydrides were present in all samples, even those with short oxidation times. Porosity mediated transitions between corrosion regimes occur at critical oxide thicknesses.





Band scan from the 80+20 day low tin ZIRLO sample

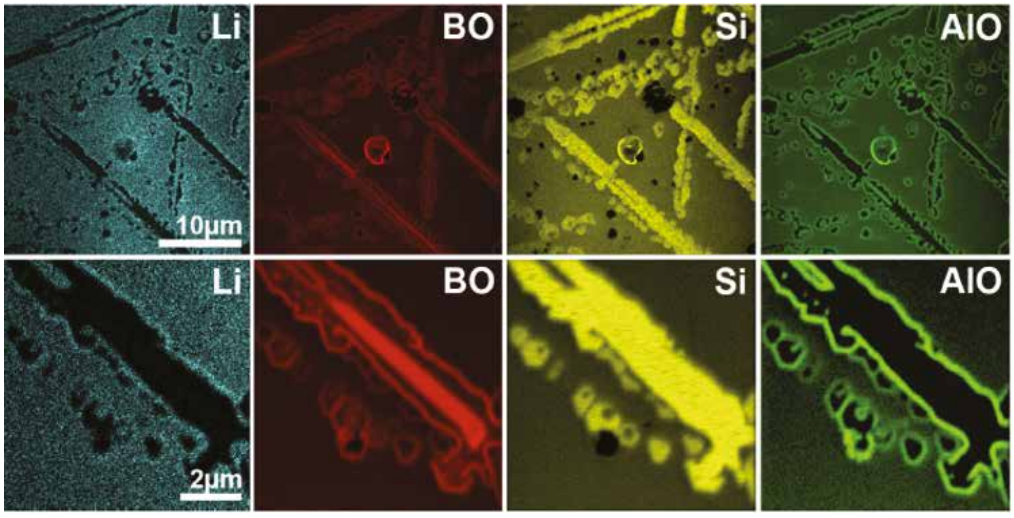
From: An investigation of the oxidation behaviour of zirconium alloys using isotopic tracers and high resolution SIMS. Sean S. Yardley et al. , Journal of Nuclear Materials 443 (2013) 436–443.

The use of an isotopically doped environment and subsequent NanoSIMS 50L analysis is a powerful methodology to study corrosion mechanisms. The ability to map large areas can give confidence on the generality of the observations.

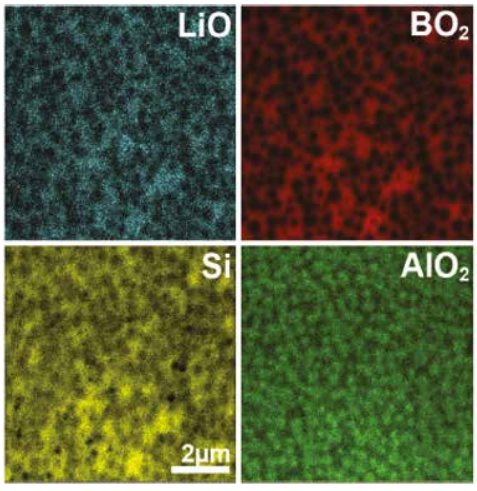
Lithium and boron analysis in glass

Glass ceramics are being developed to immobilize fission products, separated from used nuclear fuel by aqueous reprocessing, into a stable waste form suitable for disposal in a geological repository. This work documents the glass ceramic formulation at bench scale and for a scaled melter test performed in a pilot scale (1/4 scale) cold crucible induction melter (CCIM).

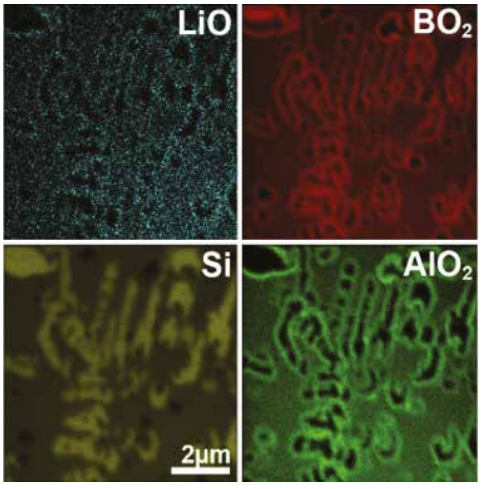
Melt viscosity, electrical conductivity, and crystallization behavior upon cooling were measured on a small set of compositions to select a formulation for melter testing. Property measurements also identified a temperature range for melter operation and cooling profiles necessary to crystallize the targeted phases in the waste form.



Finely crystalized region of the NC (no active cooling) canister specimen, at two different magnifications



Liquid-liquid phase separated region of the NC (no active cooling) canister specimen



Finely crystalized region of the NC (no active cooling) canister specimen

Cs+ primaries/negative secondary ions were used here in order to keep a good spatial resolution. Note the two sets of Secondary ions (Li^- or LiO^- , BO^- or BO_2^-, AlO^- or AlO_2^-) mentioned in the article as checks against possible mass interference ($^{27}Al^{16}O$/ $^{11}B^{16}O_2$), in fact well separated by the mass resolution of 7000) simultaneously achieved with spatial resolution and sensitivity, a uniqueness of the NanoSIMS. Since the article publication, a new RF-plasma oxygen source has been made available for O^- beam size down to 50nm. Detection of Li^+ and B^+ or BO_{2+} ions are possible with improved sensitivity and less charging issues with negative primaries.

From: Cold crucible induction melter studies for making glass ceramic waste forms: A feasibility assessment. Jarrod Crum et al. Journal of Nuclear Materials 444 (2014) 481–492.

The NanoSIMS 50L permits lithium and boron analysis in glasses.
Electrical insulators can be analyzed with metal coating and/or electron flood gun.

Ceramics: YAG (Yttrium Aluminum Garnet)

Dopant segregation imaging in two different YAG after sintering

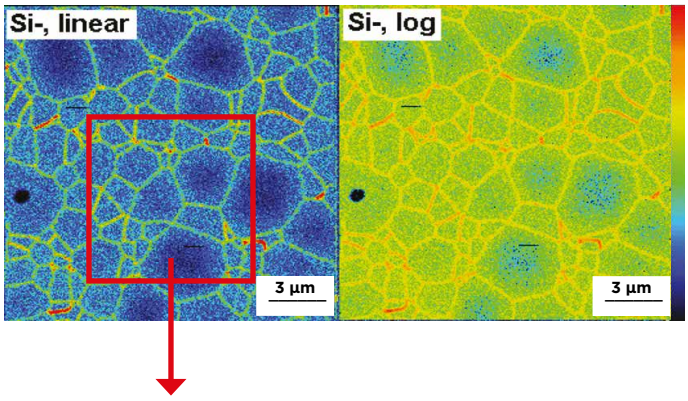
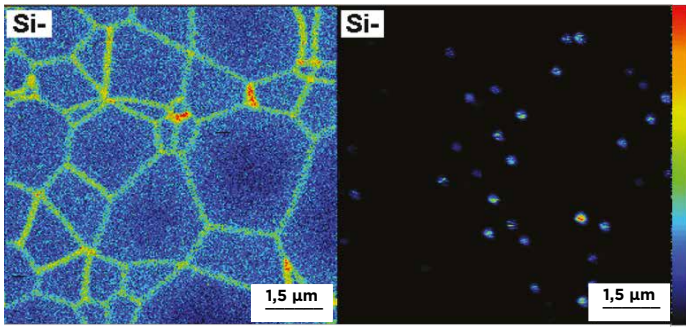


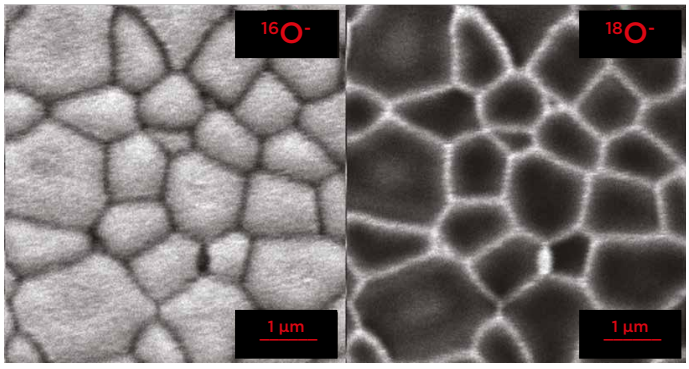
Image of the silicon **dopant** in a YAG sample (Yttrium Aluminum Garnet) in linear color scale (left) and LOG (right). The outstanding NS sensitivity leads to a high dynamic range under each pixel. LOG color scale is often used to reveal the full information. Maximum Silicon concentration at grain boundary: 0.1 at. % (<=> 50 counts).

Field of view: 20µm x 20µm.



Left: silicon dopant map zoomed from the image above. Right: the image of a different YAG sample type showing a different segregation pattern after thermal treatment (respectively grain boundary and triple points).
Field of view: 10µm x 10µm
Max Si count: 46 c/pixel
Cs+ 16 keV, , Ib: 1.5 pA, spot size: 100 nm256 x 256 pixels,
Acq: 30 min. linear display.

Use of stable isotopic tracer to study oxidation mechanism: ^{18}O at grain boundaries in sintered transparent YAG ($Y_3Al_5O_{12}$)



YAG sintered and annealed at more than 1400° Celsius under $^{18}O_2$ atmosphere.

^{16}O, original component of the oxide is replaced with ^{18}O coming from the atmosphere of the thermal treatment. The NanoSIMS permits to observe without ambiguity ^{18}O incorporation and diffusion inside the ceramics through the grain boundaries.

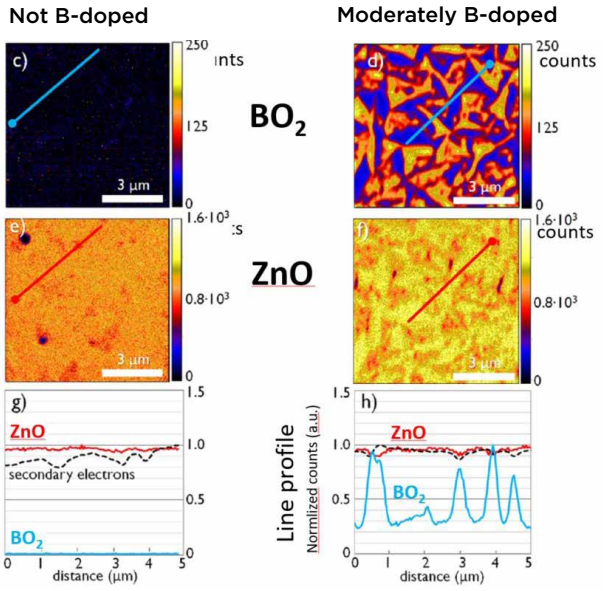
By Courtesy of Dr. Hajime Haneda and Dr Isao Sakaguchi, National Institute for Research in Inorganic Materials, Tsukuba, Ibaraki Japan.

The sensitivity required for dopant mapping is obtained with high spatial resolution and fast acquisition thanks to DC reactive primary beam and magnetic sector mass analyzer.

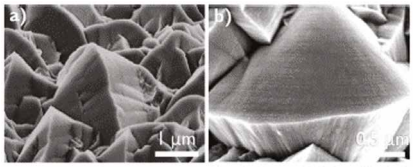
Dopant and contamination in semiconductors

Boron dopant imaging in *a*-textured polycristalline LP-MOCVD ZnO film

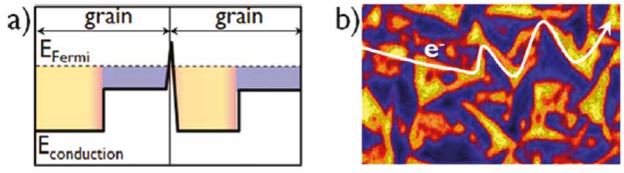
From the abstract: "Polycrystalline LP-MOCVD ZnO:B films are widely used as electrodes in copper indium gallium selenide and silicon heterojunction solar cells. (...) We unveiled a remarkable bimodal spatial distribution of B dopants using NanoSIMS and KPFM techniques. B atoms were found to be preferentially incorporated into one side of each ZnO grain. (...) the non-uniform dopant distribution locally affects the carrier concentration in the film. The microstructural difference and the observed bimodal distribution are attributed to the difference in surface termination between the two sides of each grain. By controlling the in-plane orientation of the grains, it should be possible to obtain continuously doped regions that would constitute low resistivity paths for charge carriers."



Above: NanoSIMS boron and zinc oxide maps and extracted line-scans. Left side: non-intentionally boron-doped sample. Right side: moderately boron-doped sample. The film was mechanically polished prior analysis



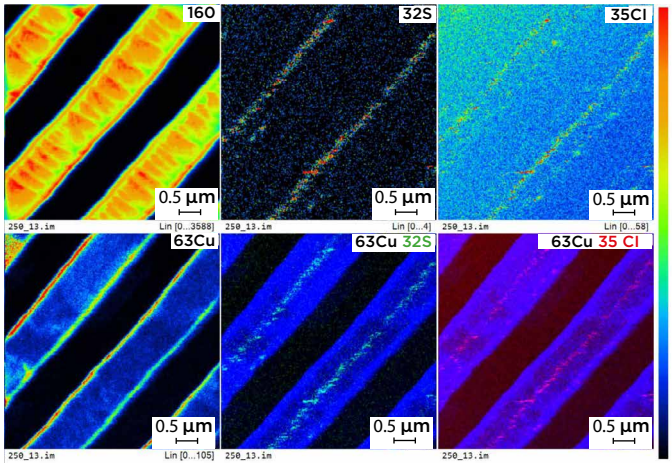
SEM view of the film grains.



(a) Electronic band diagram at a GB assuming the bimodal dopant distribution. (b) Example of an arbitrary "low resistivity" percolation path within the dopant-rich regions of the film.

From : Direct imaging of dopant distribution in polycrystalline ZnO films. Fanni Lorenzo et al. Applied Materials & Interfaces, 2 Feb 2017.

Microelectronics: S and Cl Contaminantion in copper lines after chemical mechanical polishing/planarization (CMP)



Sulphur and Chlorine, sources of corrosion, were revealed unexpectedly at the center of copper lines between silicon oxide lines. After study, the plating process used to fill the trenches was identified as responsible for this contamination. No other analytical technique could simultaneously deliver the light element sensitivity and the lateral resolution required to elucidate this problem. Simultaneous maps of carbon, oxygen, sulfur, chlorine and Copper. High mass resolution (ex: $^{32}S/^{16}O_2$ interference).

Field of view: 5µm x 5µm. Cs+, spot size: 40nm.

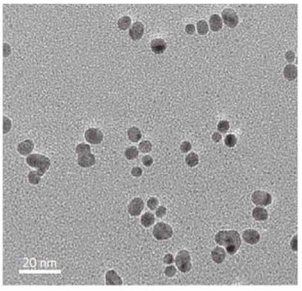
Data by courtesy of IMEC, Belgium.

The NanoSIMS 50L can contribute to the development and failure analysis in semiconductors when sub-µm resolution and sensitivity are needed together.

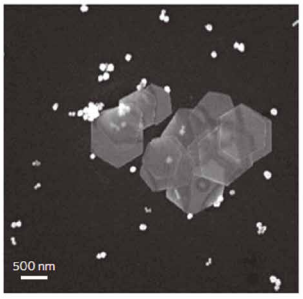
Plasmon-mediated growth of noble metal nanostructures

The role of PVP in directing the anisotropic growth of Au nanoprisms

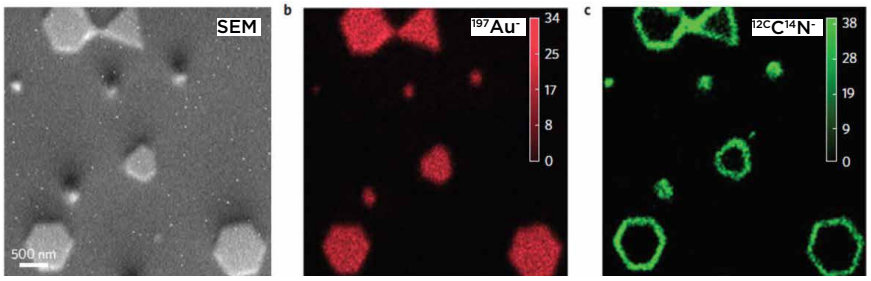
From the abstract: "...it is still unknown whether the plasmon-mediated growth of silver nanostructures can be extended to the synthesis of other noble metals. (...) Herein, we demonstrate the plasmon-driven synthesis of gold nanoprisms and elucidate the details of the photochemical growth mechanism at the single nanoparticle level. Our investigation reveals that the surfactant polyvinylpyrrolidone preferentially adsorbs along the nanoprism perimeter and serves as a photochemical relay to direct the anisotropic growth of gold nanoprisms..."



TEM of Au plasmonic seeds

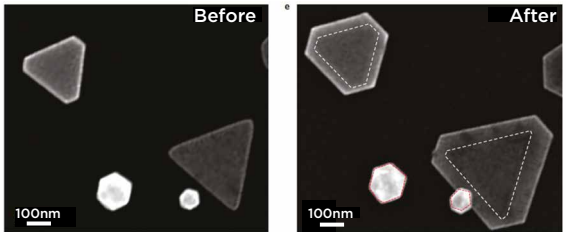


SEM of final products upon irradiation of the growth solution with 500nm light.



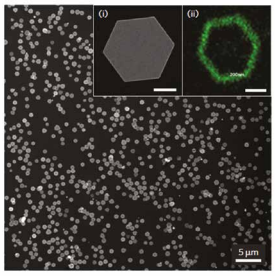
SEM, $^{197}Au^-$(red) and $^{12}C^{14}N^-$(green) NS50L images of Au nanostructures obtained after 2 h of photochemical growth. The $^{12}C^{14}N$- signals from adsorbed PVP molecules are observed along the perimeter of the planar-twinned nanoprisms and cover the entire surface of the multiply twinned nanoparticles, suggesting that twin-plane defects prompt PVP adsorption onto Au nanocrystals.

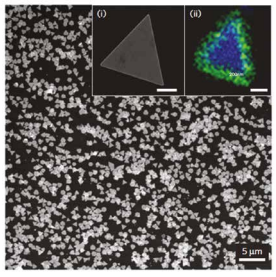
SEM images of individual Au nanoprisms and pseudo-spherical Au nanoparticles before growth (d) and after growth (e) under ~500nm light irradiation for 30 min.



Plasmon-driven synthesis of hexagonal or triangular Au nanoprisms, adding iodine

SEM image of Au hexagonal nanoprisms obtained after 2 h of irradiation following the seed separation method. Insets: high-mag. SEM image of a single hexagonal nanoprism (i) and NanoSIMS $^{12}C^{14}N^-$ image (green) from adsorbed PVP on a hexagonal nanoprism (ii).





SEM image of Au triangular nanoprisms obtained after 2 h of irradiation with the addition of iodide (I^-) to the growth solution following the seed separation method. Insets: high-mag. SEM image of a single triangular nanoprism (i) and showing NanoSIMS images of $^{12}C^{14}N^-$ (green) and $^{127}I^-$ (blue) from a triangular nanoprism (ii).

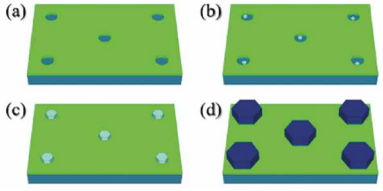
From: Polyvinylpyrrolidone-induced anisotropic growth of gold nanoprisms in plasmon-driven synthesis. Yueming Zhai et al., NATURE MATERIALS, Vol 15, August 2016.

The NanoSIMS offers a unique analytical bridge between AFM or EM (higher spatial resolution) and SIMS (higher sensitivity on larger areas), mapping simultaneous light (nitrogen) and heavy (iodine) elements.

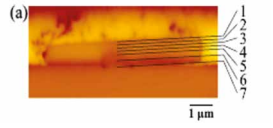
3D dopant distribution in InGaAs microdiscs grown selectively on Si (111)

The control of the dopant profile in 3-dimentional InGaAs microdiscs on Si (111) is essential for device applications. But such profiles can never be controlled by simply changing the supply of dopant precursors during the growth of microdiscs because a variety of crystal planes, such as (111), {−110}, and irregular planes near the corners, surround a hexagonal pillar of InGaAs and the incorporation efficiency of dopant elements depends on the kind of planes involved. We here observed the distributions of sulfur and zinc in p-i-n InGaAs microdiscs by both cross-sectional scanning capacitance microscopy and NanoSIMS. Even though the InGaAs shell was grown on microdiscs using dimethylzinc (DMZn), no p-type region was found on the top of the microdiscs and the p-type region existed on the sidewall of the discs alone. This suggested that the zinc incorporation efficiency on InGaAs (111) plane is much lower than that on {−110} planes. Complete encapsulation of microdiscs with p-type region was possible by post-diffusion of zinc during exposure to a mixture of tertiarybutylarsine (TBAs) and DMZn after the growth of InGaAs microdiscs.

Growth of microdiscs:
(a) 3.5-degree-off n-Si (111) substrate with patterned 100-nm thick SiO2 mask,
(b) InAs nucleation growth,
(c) InAs pillar growth, and
(d) InGaAs microdisc growth.



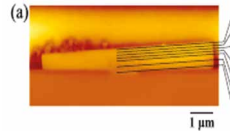
AFM of regular InGaAs µdisc section

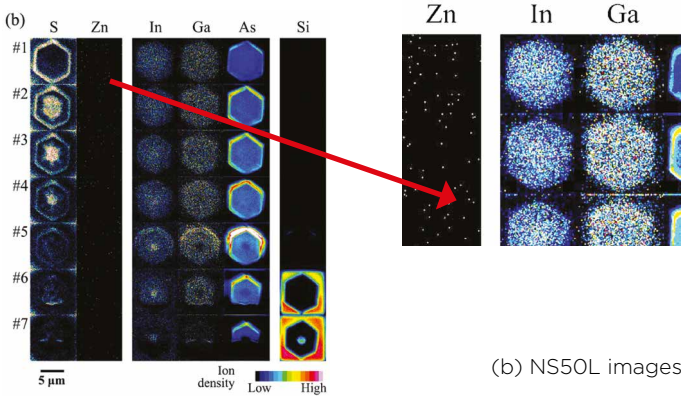


WITHOUT ZINC
post-diffusion process

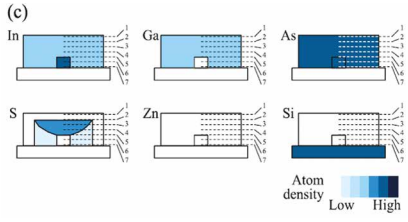
AFM of regular InGaAs µcrodisc section

WITH ZINC
post-diffusion process

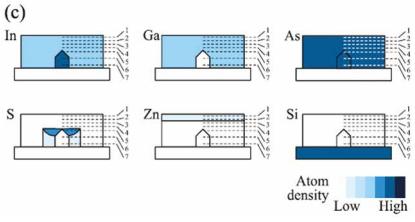




(b) NS50L images at different depths #



(c) Cross-sectional schematics of InGaAs µdisc deduced from the NS50L image stacks.



From: Measurement of 3-dimensional dopant distribution in InGaAs microdiscs grown selectively on Si (111). Tohma Watanabe et al. Journal of crystal Growth, 464, 15 April 2017.

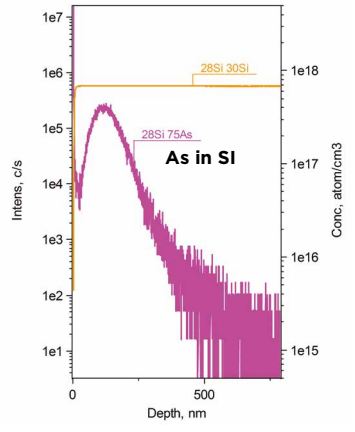
3D imaging of zinc (low ionization in SIMS) in III-V is possible in the NanoSIMS at a few hundreds nm lateral resolution and a few tens nm depth resolution.

Direct depth profiling with the NanoSIMS

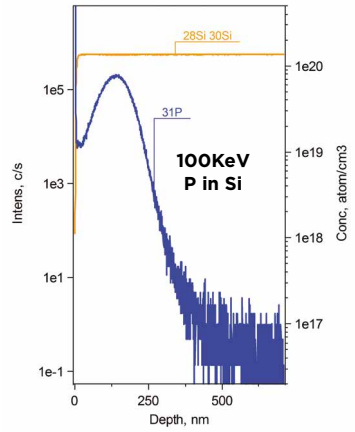
The NanoSIMS design has consequences for profiling:

- It is generally used with a relatively high impact energy of 16 keV hence depth resolution will be "moderate" (10-20nm/decade),
- Beam current varies typically between 0.5 pA and 10 nA with crater size between 1-2 µm up to 40-50µm,
- Sensitivity is high due to the high overall transmission especially at high mass resolving power and with up to seven detectors (more elements can be followed combining multicollection with B-field jumping),
- Detection limits of light elements are excellent also due to a true UHV condition (base pressure in the E-11mbar range) and good sputter speed.
- Normal incidence induces less crater bottom rugosity, full oxidation, no primary shadowing allowing profiling in holes or trenches.
- MCs^+ mode is inaccessible (need for opposite PI-SI polarities).

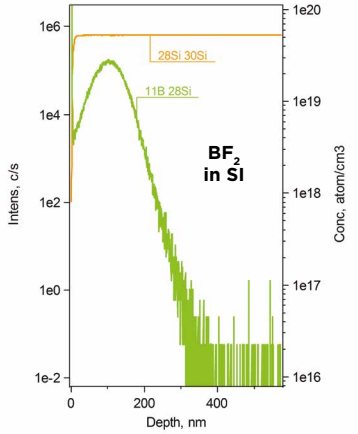
Medium size crater: Dopant implants in silicon



15x15µm, 16keV Cs+, 90 pA
Sputter rate: 8.4 nm/min (504 nm/ hour)

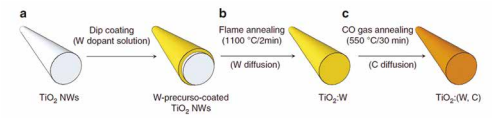


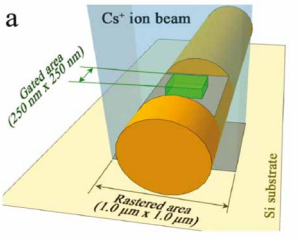
15x15µm, 16keV Cs+, 96pA
Sputter rate: 9.6 nm/min (576 nm/hour)

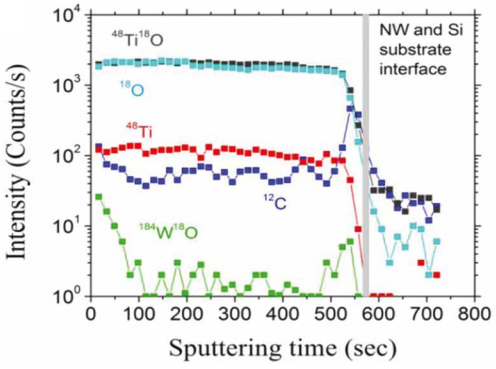


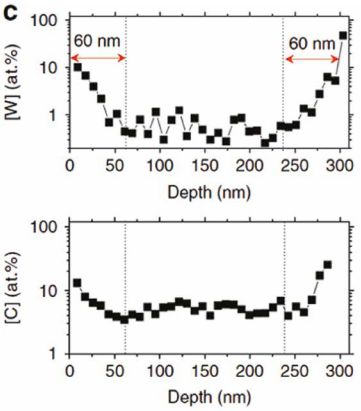
15x15µm, 16keV Cs+, 96pA
Sputter rate: 9.6 nm/min (576 nm/hour)

Small size crater: Codoping titanium dioxide nanowires with tungsten and carbon for enhanced photoelectrochemical performance









The co-doped TiO_2 nanofiber, laying flat on a substrate, is profiled perpendicularly using a small **crater size of 1 x 1µm** (electronic gate : 0.25 x x0.25 µm)

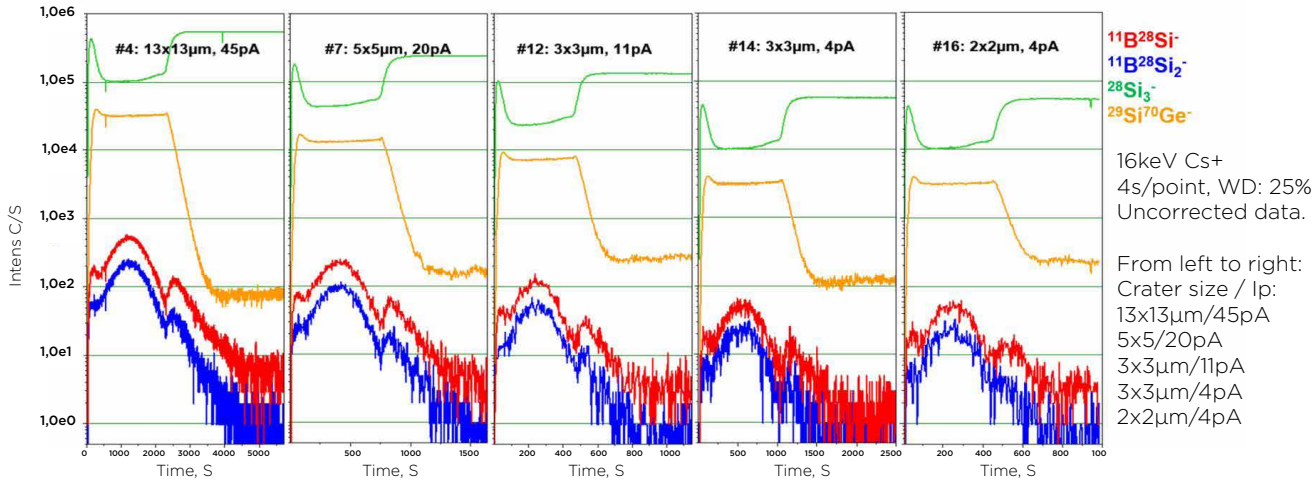
From: Codoping titanium dioxide nanowires with tungsten and carbon for enhanced photoelectrochemical performance. In Sun Cho et al., NATURE COMMUNICATIONS | 4:1723, 16 April 2013.

Direct depth profiles are possible from crater as small as 1 µm² while keeping an excellent sensitivity at high mass resolution and sub-µm beam size.

Two modes of depth profiling on the NanoSIMS

Direct profiling: initial test for self-focusing SIMS from small SiGe area

In order to analyze many 3D structures of a few nm dimensions in parallel the self-focusing methodology has been proposed [1] based on the detection of cluster ions that can originate only from the nm-structures and not the rest of the crater. For ex. measuring Ge concentration in a $Si_xGe_y^-$ finFET using $Ge_2^-/SiGe^-$ instead of Ge^-/Si^- where Si^- can come from the structure but also from the SiO_2 surrounding. Here we tested this approach applied on smaller areas in view of monitoring local loading effect (variation of device composition related to device areal density).The test sample (courtesy by INTEL) is composed of ~20nm of epitaxial Si cap followed by 200nm slightly graded 48...42 at% epitaxial SiGe layer, on Si substrate. It is doped with boron with [B]max = 2 E19 at/cm3.

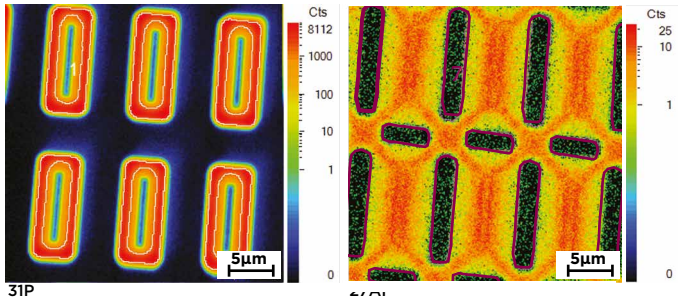


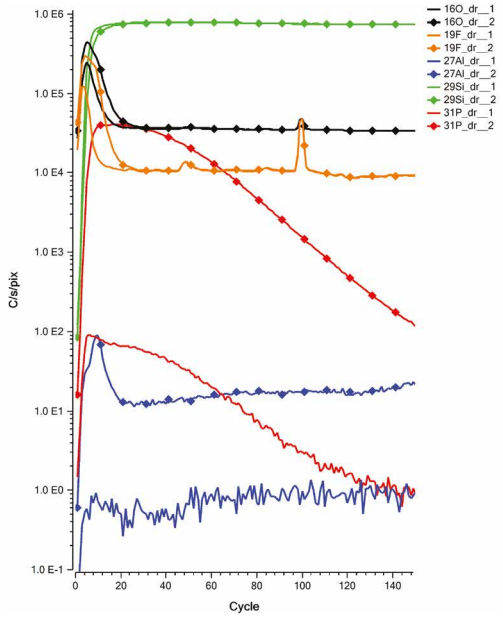
The initial test shows that the NS50L has enough sensitivity to use cluster ions technique for self-focusing mode on small craters while keeping good dopant dynamic range. More work would be needed for handling matrix effects and variation of sputter rate.

[1] W.Vandervorst, Plenary Lecture SIMS-19, Korea,2013; SIMS-20, A.Franquet et al. , Appl. Sci (2015).

Depth profile reconstruction from regions of Interest (ROIs) drawn on images

For depth profiling, the NanoSIMS 50L is also often used in image stack acquisition mode. If small details are visible, the stack can then be corrected for possible sample drift, then ROIs are drawn (manually or automatically) and depth profiles are reconstructed from the ROIs.
In the semiconductor structures below the ROI 1 is the sum of six sub-µm ROIs in white; the ROI 2 is the sum of six sub-µm ROIs in magenta. The reconstructed depth profiles are shown on the right.





The NanoSIMS permits: a) direct depth profiling, b) profile reconstruction from ROIs within image stacks, c) 3D image viewing using WinImage software.

NanoSIMS 50L






Application in Materials

Application examples and a large list of scientific articles are available from our website at www.cameca.com/products/sims/nanosims



CAMECA (Corporate Headquarters)
29 Quai des Grésillons
92622 Gennevilliers - France
Tel: +33 1 43 34 62 00
cameca.info@ametek.com

CAMECA Atom Probe Technology Center
5470 Nobel Drive
Madison WI 53711 - USA
Tel: +1 608 274 6880

www.cameca.com

B-NS-MAT-reprint-oct.-23 - Non-contractual document. CAMECA reserves the right to alter the specifications of its products without notice. All mentioned trademarks are registered by their respective owners.

WORLD PREMIER PROVIDER OF SCIENCE & METROLOGY SOLUTIONS FOR ELEMENTAL & ISOTOPIC MICROANALYSIS.
WE DELIVER CUTTING-EDGE SCIENCE AND METROLOGY SOLUTIONS, AND OFFER OUR CUSTOMERS UNPARALLELED SUPPORT AND MAINTENANCE SERVICE THROUGH THE COMPREHENSIVE AMECARE PROGRAM.

CAMECA / AMETEK
SCIENCE & METROLOGY SOLUTIONS